Comparison of vehicle-track interaction models to simulate vertical wheel/rail impact contact

Shen, Chen; Sabbatini, Luca; Wei, Zilong; Dollevoet, Rolf; Li, Zili

Publication date
2018

Document Version
Accepted author manuscript

Published in
Dynamics of Vehicles on Roads and Tracks

Citation (APA)
Shen, C., Sabbatini, L., Wei, Z., Dollevoet, R., & Li, Z. (2018). Comparison of vehicle-track interaction models to simulate vertical wheel/rail impact contact. In M. Spiryagin, T. Gordon, C. Cole, & T. McSweeney (Eds.), *Dynamics of Vehicles on Roads and Tracks: Proceedings of the 25th International Symposium on Dynamics of Vehicles on Roads and Tracks (IAVSD 2017), 14-18 August 2017, Rockhampton, Queensland, Australia* (Vol. 2, pp. 1-7). CRC Press.

Important note
To cite this publication, please use the final published version (if applicable).
Please check the document version above.

COMPARISON OF VEHICLE-TRACK INTERACTION MODELS TO SIMULATE VERTICAL WHEEL/RAIL IMPACT CONTACT

Chen Shen, Luca Sabatini, Zilong Wei, Rolf Dollevoet and Zili Li
Faculty of Civil Engineering and Geosciences, Delft University of Technology
Stevinweg 1, 2628 CN Delft, the Netherlands
C.Shen-2@tudelft.nl

ABSTRACT: This study compares various assumptions in different models to assess their capabilities to model vehicle-track interactions up to 2 kHz at a single rail-top defect. Field measurement data are used to evaluate discrepancies. The characteristics of contact force and axlebox acceleration (ABA) are first identified and qualitatively correlated with track, wheelset and contact models. Subsequently, the results from different models are quantitatively compared in terms of their capabilities to reproduce those characteristics. It is found that the differences in sleeper and wheel-rail contact models lead to the most significant discrepancies. The causes and physical implications of the quantified discrepancies are also discussed.

1 INTRODUCTION

Wheel-rail vertical impact usually occurs when short wavelength defects (e.g., squats, poor welds, wheel flats, short-pitch corrugations) or structure discontinuities (e.g., insulated joints, crossings) are present. To investigate the dynamic behavior of vehicle-track interaction upon impact, various models exist, incorporating different simplifications and assumptions (Knothe & Grassie 1993). These assumptions will inevitably cause discrepancies in the simulation results obtained from different models and between the simulation results and measurement data. Therefore, there is a need to compare different models and quantify the effects of their different assumptions on the simulation results.

Benchmark tests are usually designed to compare the capabilities of different models in different wheel/rail impact scenarios, e.g., corrugation (Grassie 1996), wheel flat and dipped joint (Steffens 2005). However, in addition to different assumptions, of which there are often more than one between two benchmark participants, models may differ in their solution techniques and input requirements. Thus, it is difficult to determine exactly which assumption contributes to an identified discrepancy. Alternatively, comparative studies can be carried out by using models that vary only in their assumptions of interest, e.g., track flexibility (Di Gialleonardo et al. 2012), wheelset flexibility (Nielsen 2008) or contact models (Burgelman et al. 2015). However, comparative studies are, in most cases, less comprehensive than benchmark tests in terms of the number of model types and the simulated cases involved. This undermines the generality of their conclusions. In addition, suitable metrics that can reflect the correlation between two sets of results are still to be defined for quantification. With these issues remaining unaddressed, up till now, there is no quantifiable conclusion on how each model assumption would influence the simulation results in a wide variety of impact scenarios.

The objectives of this paper are therefore (1) to identify and quantify the effects of different model assumptions on simulation results and (2) to better understand the causes and physical implications of the quantified discrepancies.

2 METHOD

Two types of models are compared: Model A uses a two-layer discretely supported beam model to represent the track and a rigid mass to model the wheelset, as shown in Figure 1a, and Model B employs a detailed three-dimensional finite element (FE) model meshed with solid elements for both track and wheelset. For both models, only halves of the track and wheelset are considered. The bogie and carbody are simplified as sprung masses. The railpads and ballast are modelled as discrete spring-damper pairs. The rail and sleeper models compared are listed in Table 1. Four different contact models are also compared. The two simplest contact models are linear and non-linear Hertzian spring models, for which the half-space assumption applies. To account for local geometric variations within the contact area in the longitudinal direction, a two-dimensional model with multiple independent springs along the longitudinal direction is considered, referred to as the Winkler bedding model. The aforementioned three contact models are implemented in model A; see Figure 1a. In addition, a three-dimensional FE contact model that considers real contact geometries (Molodova et al. 2014) is implemented in model B.

An actual wheel/rail impact case caused by a short wavelength rail top defect (Molodova et al. 2014) is simulated using the different models. The location and longitudinal geometry of the defect, denoted as $Z_{irr}(x)$, are shown in Figure 1c. The model parameters used in this paper are the same as those used in (Molodova et al. 2014). Measured vertical axle box acceleration (ABA) is also used for comparison. As Model B2 has been validated in (Molodova et al. 2014) with ABA, it can serve as a reference.

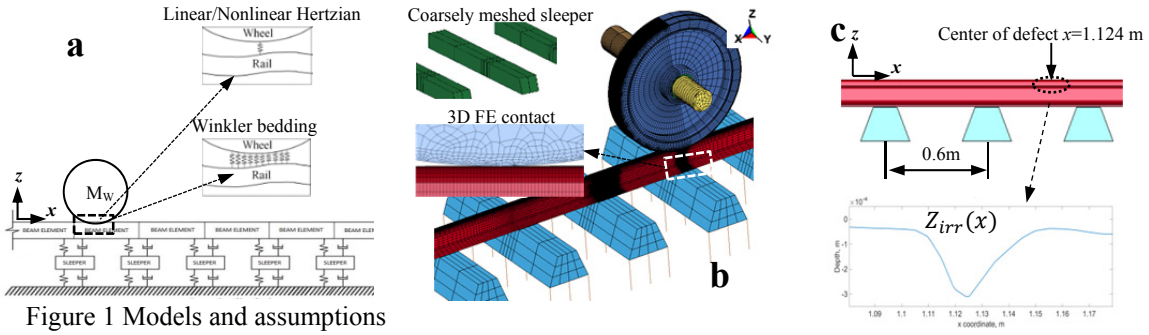

Figure 1 Models and assumptions

Table 1 Track Models and their assumptions to be compared

Model	A					B		
	1	2	3	4	5	1	2	3
Rail	E-B	T	E-B	T	T	FE	FE	FE
Sleeper	Rigid	Rigid	E-B	E-B	T	Rigid	Coarse Mesh	Fine Mesh

Note: E-B stands for Euler-Bernoulli beam; T stands for Timoshenko beam

3 RESULTS

3.1 *Characteristics of contact force and ABA*

Figure 2 shows the results from the reference FE model and measured ABA. Time domain signals (Figure 2 a, c) can be divided into two phases. From 1.1 m to approx. 1.15 m, the wheel-track system is in a forced vibration phase, with external excitation being the irregularity (see the geometry in Figure 1c). System responses can be described as a local minimum (D1) followed by a local maximum (M1). From 1.15 m on, the system is in a free vibration phase. The time domain signals can be decomposed into two major oscillatory modes: one is defined by the wave pattern between the local maxima M1, M2, M3, and so on, and the other, which has a longer wavelength, is defined by the wave pattern between the local minima D1, D2, D3, etc., leading to two major characteristic frequencies around 1050 Hz and 270 Hz, as shown in Figure 2b, d. For the calculated contact force, vibration energy is higher at 270 Hz than at 1050 Hz, whereas for both the calculated and measured ABA, energy predominates at 1050 Hz.

3.2 *Correlating characteristics to the wheel-track system*

To qualitatively illustrate the correlations between the characteristics in 3.1 and the wheel-track system, the direct receptance of the track, wheelset and contact at the impact location is employed to represent system characteristics, as shown in Figure 3c. Track receptance is obtained by simulating a hammer test on the reference FE model. For simplicity, wheelset receptance is calculated with a rigid mass of 900 kg (half of a motorized wheelset), and contact receptance is obtained using a spring with a linearized stiffness of $1.1 \times 10^9 \mathrm{N/m}$. The effects of the wheelset flexibility and contact nonlinearity are discussed later in this section.

The two major oscillatory modes identified in the contact force and ABA correspond to the two resonances of the wheel-track system, which can be identified by the intersection points of the mass-lines and stiffness-lines in Figure 3c, as in a single degree of freedom mass-spring system. This correlation is further demonstrated later, in Section 3.3, with the different models. For the current system, two straight mass-lines are derived by fitting to the track receptance curve (see ML1 and ML2 in Figure 3c). These lines intersect the stiffness-line of the contact spring at 270 Hz and 1050 Hz (see the green dots), thus indicating the two resonance modes of the coupled track mass and contact spring. For both modes, the wheelset can be considered immobile in the vertical direction because it has a much lower receptance than the other two components. The effective masses represented by ML1 and ML2 are 386 kg and 25 kg, respectively. Therefore, the wheel-track system behaves as would a mass of 386 kg with the contact spring stiffness at 270 Hz and a mass of 25 kg with the contact spring stiffness at 1050 Hz. It should be noted that these two modes are by nature not the anti-resonances (e.g., the anti-sleeper or pin-pin resonance) of the track. It is also interesting to note that the track resonances measured at the impact location correspond closely to the dips (anti-resonances) of the system response, as indicated by the blue dots in Figure 3c, e, respectively.

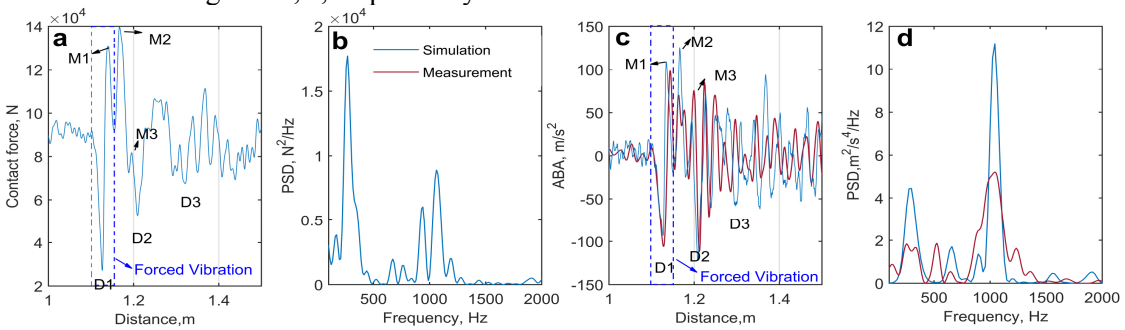

Figure 2. Characteristics of the contact force (a, b) and ABA (c, d)

The energy distribution of the contact force at different frequencies depends on two factors. The first is the input excitation energy of the system, denoted by $X(\omega)$. For a singular rail top defect, its excitation energy acts as a lowpass filter (Figure 3a). The other determinant is the capability of the wheel-track system to transfer input energy to contact force energy, which is usually defined by a transfer function $H(\omega)$. Figure 3d shows the $H(\omega)$ calculated by the receptance of the wheel, track and contact (Thompson 2009). The response energy can then be estimated by $Y(\omega) = H(\omega)X(\omega)$. As shown in Figure 3d, the current wheel-track system tends to distribute more energy in the high-frequency mode. However, due to the low-pass filter effect of $X(\omega)$, the response energy at around 1050 Hz is partly attenuated, making it lower than that around 270 Hz, as shown in Figure 2b and Figure 3e.

For the energy distribution of the ABA, the wheelset resonances must also be considered. It can be seen from the wheelset receptance (Figure 3b) that there are two narrow banded resonances for the flexible wheelset, at 400 Hz and 1000 Hz. As a result, the energy of the high-frequency mode in Figure 2f is boosted to be higher than that of the low-frequency mode, as the higher characteristic frequency coincides with one of the wheelset resonances. It should also be noted that a linearized contact stiffness is assumed here. In reality, the contact stiffness varies with the magnitude of the contact force (load-dependency). This manifests as vertical translations of the contact receptance line in Figure 3a, intersecting with the track receptance curve at different points.

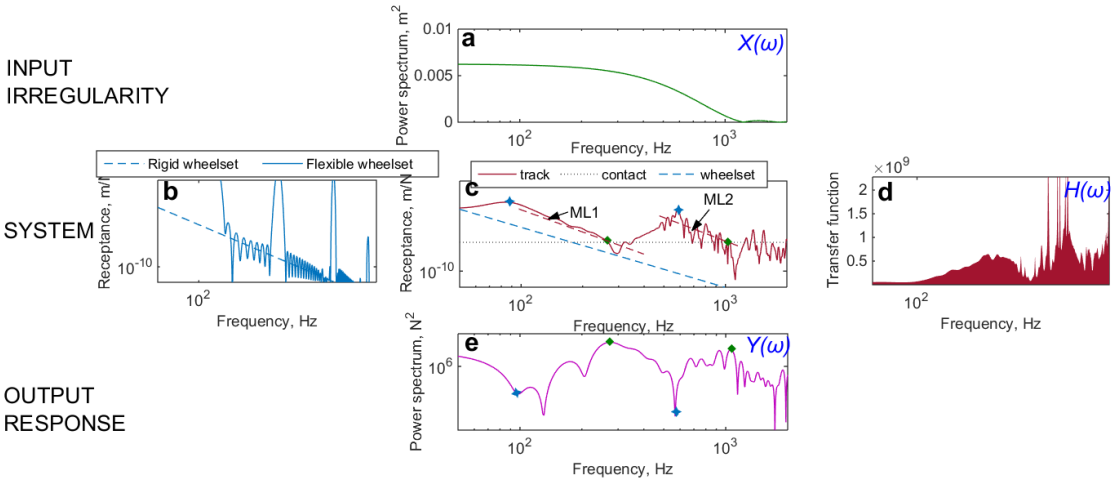

Figure 3. Correlations among input, characteristics of wheel-track system and output

3.3 *Influences of different model assumptions*

3.3.1 *Influences of the rail models*

The contact forces calculated using Models A1 (E-B beam), A2 (Timoshenko beam) and B1 (solid element) are used to demonstrate the influence of different rail models. In these models, sleepers are represented by rigid masses, so their influences can be eliminated. The track receptances of the three models are shown in Figure 4c. Models A2 and B1 have a relatively similar track receptance up to 800 Hz, whereas that of A1 deviates from the other two above 500 Hz. Below 500 Hz, the track receptances of the three models intersect with the contact receptance closely at about 430 Hz, 400 Hz and 380 Hz for A1, A2 and B1 (see Figure 4e), respectively, thus matching the characteristic frequencies of the lower frequency oscillatory mode (see Figure 4b). For the higher characteristic frequencies, those of A2 and B1 are close to each other at 1130 Hz and 1160 Hz, respectively, whereas that of A1 occurs around 1350 Hz. This finding implies that the E-B beam is not suitable for rail models for high-frequency responses.

The maximum dynamic loads are approximately 2.7 and 1.8 times the static load for the beam models (A1 and A2) and solid FE model (B1), respectively. This can be explained by the energy distribution of the wheel-track system from two perspectives. With the solid FE model, the system tends to transfer more energy to the low-frequency mode (Figure 4d), whereas with the beam models, more energy is trapped at the high-frequency mode, resulting in a larger power magnitude at the higher frequency mode (Figure 4c) and, thus, larger impact forces. Such characteristics of energy transfer are closely related to the relative phase angle between different system components. Additionally, as loss of contact occurs in A1 and A2, during which more kinematic energy will be gained due to the unconstrained rebound of the rail and sleeper, the impact velocity and, thus, the excitation energy X(ω) to the wheel-track system upon impact are higher than those in B1. This leads to a higher response energy Y(ω) in A1 and A2 than in B1 at the lower frequency mode, as shown in Figure 4b (which would otherwise have been lower based merely on the transfer function H(ω) in Figure 4d), and consequently also contributes to a larger impact force.

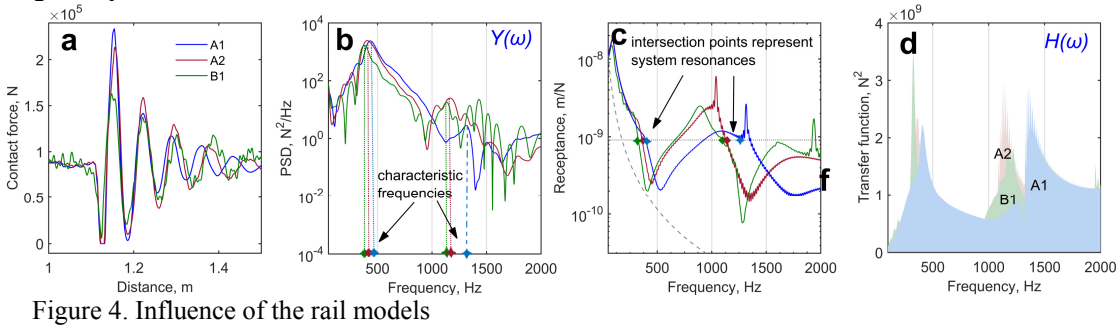

Figure 4. Influence of the rail models

3.3.2 *Influences of the sleeper models*

In this section, the sleeper models are varied: Models A2 (sleeper modeled as a rigid mass), A4 (E-B beam), A5 (Timoshenko beam), B2 (solid element with coarse mesh) and B3 (solid element with fine mesh) are compared in Figure 5. Obviously, the rigid sleeper model (A2) deviates greatly from the other models. The lower characteristic frequency of A2 is at 400 Hz, whereas that of the others occurs around 270 Hz; see Figure 5 b. The higher frequency mode of A2 is above 1000 Hz, and its vibration energy is much smaller than that of the lower frequency mode. This occurs because the wheel-track system with rigid sleepers is inclined to distribute more energy to the low-frequency mode as opposed to that with flexible sleepers, as shown in Figure 5d. Consequently, the power magnitude of A2 at low frequency mode is much larger, corresponding to a much larger dynamic load than in the other models.

In Figure 5c, the track receptances of the beam models (A4 and A5) and solid FE model (B3) are comparable below 800 Hz, which is also observed in the rail modeling. Additionally, similar to the rail models, the beam models generate slightly higher characteristic frequencies than does the solid FE model at both oscillatory modes, see Figure 5b. The differences between the Timoshenko and E-B beam for sleeper modeling seem to be marginal compared to the differences observed for rail modeling. In terms of the energy distribution of the contact force, the beam models deliver a much larger power magnitude than the solid FE model at the higher frequency mode (see Figure 5b). Such a large discrepancy is induced by the effect of contact loss, as explained earlier. Meanwhile, at the lower frequency mode, the power magnitudes of the beam models are only slightly larger than that of the solid FE model (see Figure 5b). Correspondingly, the resultant contact forces of the beam models are also only slightly larger than that of the solid FE model, as shown in Figure 5a. This occurs because in the current case, the contact forces are dominated by the low-frequency mode.

None of the models produced results that are close to those of the reference model B2. Even for the two solid element models, i.e., B2 and B3, noticeable discrepancies are observed. These discrepancies are due to the control technique used for the solid finite elements. To guarantee the computational efficiency of B2 and B3, reduced integration is used for the elements. Non-physical deformation modes with zero strain energy, referred to as hourglass modes, have to be properly controlled for this type of element. For a coarsely meshed model, especially as in B2, where only one layer of the element is meshed for modeling the bending behavior of the sleepers, enhanced hourglass control is needed to calculate the contact force. If the same amount of hourglass control is used for fine meshes, as in B3, it may over-stiffen the model.

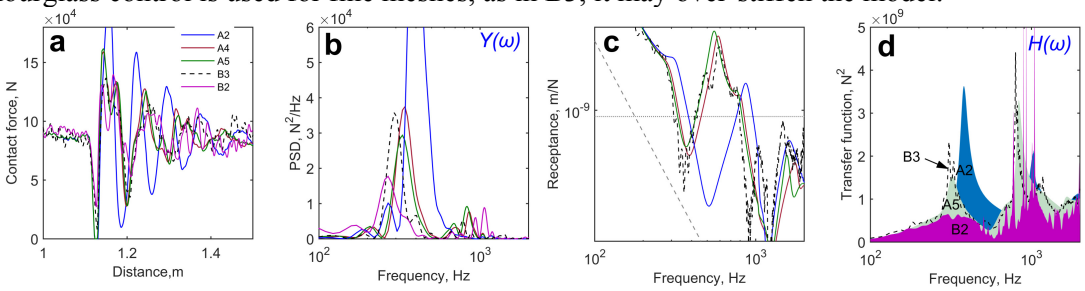

Figure 5. Influence of the sleeper models

3.3.3 *Influence of contact models*

In Figure 6a, as the contact model changes from 3D FE model to 2D Winkler bedding model and further to 1D Hertzian spring model, the dropping rate of the contact force in the forced vibration phase becomes larger, resulting in contact loss in the 1D and 2D models. The linear and non-linear Hertzian spring models yield nearly identical results, whereas the results from the Winkler bedding model show slightly lower energy in both oscillatory modes; see Figure 6b. Compared to the other three models, the 3D FE contact model creates even lower energy in the high-frequency mode. Such an increase in energy in the case of contact loss has already been discussed in 3.3.1.

In fact, the loss of contact is closely related to the differences in the contact models. The advantage of the 3D contact model is that it can correctly model the local elastic deformation on the rail surface due to wheel-rail contact; see Figure 6c. Therefore, as the wheelset position moves from x1 to x2, the deformation calculated by the 3D model will not fully recover due to

the inertia of the deformed material. Thus, the new contact force at x2 will be calculated based on the irregularity plus the residual deformation at x1. In this manner, the rate of change of the vertical irregularity $\dot{Z}_{irr}(x)$ is effectively reduced; see, for example, the blue line (with local deformation) compared to the cyan line (original geometry) in Figure 6c. However, in the 1D and 2D models, local deformation is modeled as springs. As the spring is massless, it immediately reverts to its initial or nominal length once the wheel is at x2; therefore, no deformation information from x1 is preserved. The calculation of contact force at x2 will be based only on the geometry of the irregularity. Such influence due to the inertia of the contact model becomes more pronounced if the excitation energy is trapped at higher frequencies and the amplitude of the irregularity is closer to the amplitude of the local elastic deformation.

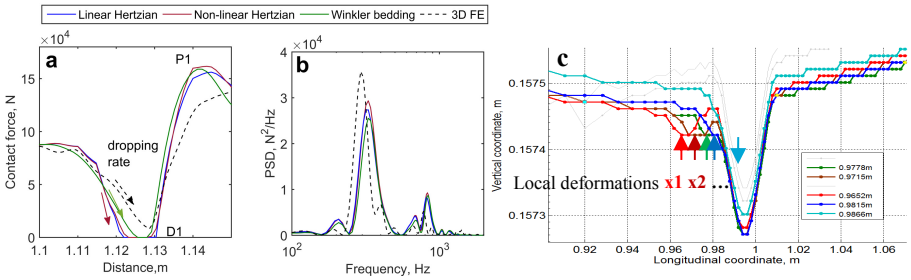

Figure 6. Influence of the contact models

4 CONCLUSION

- The system response of wheel/rail impact due to a singular rail top defect is characterized by two oscillatory modes; they are, by nature, coupled system resonances instead of the resonances or anti-resonances of the track alone.
- Compared to the solid FE model, the beam and rigid mass models tend to shift the characteristic frequencies to higher values and overestimate the power magnitude of the impact force at both oscillatory modes. More rigid rail model tends to trap the energy in the high frequency mode, while more rigid sleeper model will distribute more energy in the low frequency mode. They both lead to an overestimation of the resultant contact force.
- The rigid sleeper model and Euler-Bernoulli rail beam model produce the largest discrepancies. Such differences will be narrowed with the Timoshenko rail beam model, whereas the Timoshenko or E-B sleeper beam model, in combination with the Timoshenko rail beam model, will yield the best match with the solid FE model.
- Contact loss leads to a higher input energy to the system and, thus, to a higher impact force. Being able to consider inertia in the contact model will avoid an unrealistic loss of contact and will thus avoid overestimating the contact force.

REFERENCES

Burgelman, N. et al., 2015. Influence of wheel–rail contact modelling on vehicle dynamic simulation. *Vehicle System Dynamics*, 53(8), pp.1190–1203.

Di Gialleonardo, E., Braghin, F. & Bruni, S., 2012. The influence of track modelling options on the simulation of rail vehicle dynamics. *Journal of Sound and Vibration*, 331(19), pp.4246–4258.

Grassie, S.L., 1996. Models of Railway Track and Vehicle/Track Interaction at High Frequencies: Results of Benchmark Test. *Vehicle System Dynamics*, 25(sup1), pp.243–262.

Knothe, K.L. & Grassie, S.L., 1993. Modelling of railway track and vehicle/track interaction at high frequencies. *Vehicle System Dynamics*, 22(3–4), pp.209–262.

Molodova, M. et al., 2014. Validation of a finite element model for axle box acceleration at squats in the high frequency range. *Computers and Structures*.

Nielsen, J.C.O., 2008. High-frequency vertical wheel-rail contact forces-Validation of a prediction model by field testing. *Wear*, 265(9–10), pp.1465–1471.

Steffens, D.M., 2005. *Identification and Development of a Model of Railway Track*. Queensland University of Technology.

Thompson, D., 2009. Wheel/Rail Interaction and Excitation by Roughness. In *Railway Noise and Vibration*. pp. 127–173.